Published in final edited form as:
Nat Cell Biol. 2010 January ; 12(1): 60–9. doi:10.1038/ncb2005.

An actomyosin-based barrier inhibits cell mixing at compartmental boundaries in *Drosophila* embryos

Bruno Monier[#1,*], **Anne Pélissier-Monier**[#1,2], **Andrea H. Brand**[1,2], and **Bénédicte Sanson**[1,*]

[1]Department of Physiology, Development and Neuroscience, University of Cambridge, Downing Street, Cambridge CB2 3DY, UK.

[2]The Gurdon Institute, University of Cambridge, Tennis Court Road, Cambridge CB2 1QN, UK

[#] These authors contributed equally to this work.

Abstract

Partitioning tissues into compartments that do not intermix is essential for the correct morphogenesis of animal embryos and organs [1-3]. Several hypotheses have been proposed to explain compartmental cell sorting, mainly differential adhesion [1-9] but also cytoskeleton [10,11] or cell proliferation [10,12] regulation. Nevertheless, the molecular and cellular mechanisms that keep cells apart at boundaries remain unclear. Here we demonstrate in early *Drosophila* embryos that actomyosin-based barriers stop cells from invading neighbouring compartments. Our analysis shows that cells can transiently invade neighbouring compartments, especially when they divide, but are then pushed back into their compartment of origin. Actomyosin cytoskeletal components are enriched at compartmental boundaries, forming cable-like structures when the epidermis is mitotically active. When MyoII function is inhibited, including locally at the cable by Chromophore-Assisted Laser Inactivation (CALI) [13,14] in live embryos, dividing cells are no longer pushed back, leading to compartmental cell mixing. We propose that local regulation of actomyosin contractibility, rather than differential adhesion, is the primary mechanism sorting cells at compartmental boundaries.

Keywords

Cell sorting; lineage restriction; parasegment; boundary; compartment; non-muscle Myosin II; actin cytoskeleton; Chromophore-Assisted Laser Inactivation (CALI)

During animal development, discrete developmental units called compartments are separated by boundaries of lineage restriction that stop cells with different identities from mixing. In addition, compartmental boundaries often localise signalling centres. Segregating cell populations at compartmental boundaries is therefore essential for the correct patterning and differentiation of surrounding tissues [1-3]. This organising principle is conserved from flies to humans, where cell sorting defects during compartmentalisation are thought to cause

[*]Correspondence should be addressed to BS (bs251@cam.ac.uk) and about CALI to BM (bm343@cam.ac.uk) .

Supporting Online Material Materials and Methods Figs. S1 to S6 Movies S1 to S3

Competing financial interests The authors declare that they have no competing interests.

Europe PMC Funders Author Manuscripts

malignant invasion and congenital defects such as cranio-fronto-nasal syndrome [15-17]. In the vertebrate hindbrain rhombomeres and in the *Drosophila* wing disc, cell sorting between compartments is governed both by transcription factors that confer compartment specific identities and by signalling localised at the boundaries, such as EPH/Ephrin, Hedgehog or Notch signalling [4,18-26]. Downstream of these factors, several mechanisms have been proposed to explain cell sorting, mainly differential adhesion [1-9] but also regulation of the cytoskeleton [10,11], regulation of cell proliferation [10,12] or extracellular matrix fences [3]. However, support for these hypotheses is scarce *in vivo* and the molecular and cellular mechanisms sorting cells at compartmental boundaries remain unclear.

Here, we investigate this problem in the early *Drosophila* embryo. During segmentation, the trunk is divided into alternating anterior and posterior (A/P) compartments (Fig. 1a) [27]. Anterior cells expressing the Wnt-1 homologue Wingless (Wg), and posterior cells expressing the homeodomain protein Engrailed (En), are separated by parasegmental (PS) boundaries, which behave as boundaries of lineage restriction (they stop cell mixing) during stages 8-11 [28]. The posterior interface of the Engrailed stripe (where the segment border will form later in embryogenesis), is not a barrier to cell mixing [28].

We found that during stages 8-11, cells on both sides of the PS boundary minimize their contacts, forming a straight line of adjoining membrane interfaces (Fig. 1b). When compartmentalisation is compromised, as in *wingless* mutants, membrane alignment is lost and some cells invade the opposite compartment (Fig. 1c). We have quantified the degree of misalignment by measuring an index of straightness (IS) for a row of interfaces: the straighter the row, the closer the IS to 0, which corresponds to a straight line. Quantification confirms that PS boundaries interfaces are significantly straighter than other dorso-ventral columns of interfaces that are not PS boundaries (IS=3.7±0.4 for PS boundaries, IS=14.2±1.1 for other interfaces, n=25) (Fig. 1d). In wg^{CX4} mutant embryos, the interfaces that should have formed PS boundaries have an IS of 14.8±1.0 (n=24), which is similar to non-boundary interfaces in wild-type (Fig. 1d). We conclude that membrane alignment is a property of lineage restriction boundaries in the *Drosophila* embryo.

To identify effector genes required for cell sorting at PS boundaries, we screened for genomic deletions that cause altered *en* expression pattern. We recovered several deletions giving embryos with irregular boundaries reminiscent of loss-of-compartmentalisation phenotypes (Fig. S1). Several of these deletions remove at least one regulator of the Wingless signalling pathway, consistent with its role in A/P compartmentalisation. One small deletion, however, does not remove known Wingless pathway components, but removes one of the two cytoplasmic *actin* genes (*actin5C*) as well as *spaghetti-squash* (*sqh*), which encodes the non-muscle Myosin II Regulatory Light Chain (MRLC). To test a potential role of the actomyosin cytoskeleton in lineage restriction at PS boundaries, we assayed membrane alignment in embryos in which non-muscle Myosin II (MyoII) function is disrupted. Embryos homozygous for null alleles of *zipper*, which encodes the Myosin Heavy Chain (MHC), do not exhibit irregular PS boundaries (not shown), presumably because maternal pools of MHC are sufficient to provide function. To target both maternal and zygotic pools of MyoII, we treated embryos with the drug, Y27632, which inhibits MRLC by preventing its phosphorylation by its upstream activator Rho kinase. Injection of

Y27632 into early embryos, at a dose where the epithelium remains intact and cell divisions are still happening, disrupts membrane alignment at PS boundaries (IS=10.4±1.9, n=26 compared to IS=4.3±0.4, n=25 in H_2O-injected embryos) (Fig. 1d, e). The invasion of single cells from A or P compartment into the adjacent compartment is observed (Fig. 1e). PS boundary defects in Y27632-treated embryos are caused by specific inhibition of MyoII, since these can be rescued by expressing a constitutively active E20E21 phosphomimetic form of MRLC, $MRLC^{E20E21}$, which functions in the absence of Rho kinase (IS=5.0±0.8, n=26) (Fig. 1d, e). Similar cell sorting defects are found when embryos express dominant negative forms of MHC (IS=10.3±1.4, n=25, for DN-MHC^{YFP} expressed from an endogenous promoter, and IS=13.9±1.0, n=23 for UAS-DN-MHC^{GFP} expressed with *arm*Gal4VP16) (Fig. 1d and Fig. S2). Thus, inhibiting maternal and zygotic pools of MyoII, either by drug injection or by expression of dominant-negative forms, gives rise to cell sorting defects similar to the loss of A/P compartmentalisation in *wingless* mutants. We conclude that a functional actomyosin cytoskeleton is required for lineage restriction at PS boundaries.

To investigate how the actomyosin cytoskeleton controls lineage restriction, we looked at the sub-cellular organisation of filamentous actin and MyoII in boundary cells. MyoII (and F-actin to a lesser extent) is enriched at cell-cell interfaces at the PS boundary, forming a linear cable-like structure (Fig. 2a and Fig. S3b-c), similar to the enrichment reported recently for the wing disc D/V boundary [10,11]. We did not observe any difference in the structure of the PS MyoII enrichments between parasegments or between ventral, lateral or dorsal ectoderm (Movie S1 and data not shown). The PS MyoII cable, similarly to planar MyoII enrichment observed at stage 6 to 8 during germ-band extension [29], is contributed by both anterior and posterior cells, since the PS MyoII enrichment is observed at the posterior junction of *wg*-cells and at the anterior junction of *en*-cells (Fig. 2d and S3d). The presence of the PS MyoII cables corresponds to the period of lineage restriction at PS boundaries in wild-type embryos (stages 8-11, Fig. S3a). The Myo II cable is located at the level of the adherens junctions (AJs) (Fig. 2a and Fig. S3e, f), which is where membranes are aligned at the PS boundary (IS=3.6±0.7 at AJs and IS=10.5±0.9 5μm below AJs, n=8) (Fig. 2c, Fig. S3f, g). In addition, the cable is absent in the compartmentalisation mutant wg^{CX4} (Fig. 2b). We conclude that lineage restriction at PS boundaries correlates with the presence of a specialised actomyosin structure at the apical cortex of boundary cells (Fig. 2e).

To understand how this cable could promote cell sorting at PS boundaries, we looked at cell behaviours close to the boundaries in live embryos, using MRLC-GFP (Movie S1). We found that the PS boundary can be transiently deformed by the division or, more rarely, by the intercalation of boundary cells (Fig. 3a, b and Fig. S4a). During these events, the MyoII cable is not dismantled (Fig. 3a, b and Fig. S4). When a dividing boundary cell rounds up and transiently invades the adjacent compartment, the MyoII cable at the boundary cortex deforms strongly (Fig. 3c, c' and Movie S2). Approximately when cytokinesis starts, the MyoII cable straightens out and the daughter cells go back to their compartment of origin. This suggests that the MyoII cable corrects cell mixing by providing a barrier of cortical tension at boundary interfaces.

To test this hypothesis, we developed a method to specifically inhibit MyoII function in PS boundary cables in live embryos. Chromophore-Assisted Laser Inactivation (CALI) has been used in cultured cells to inactivate single proteins with sub-cellular resolution, including myosins [13,14,30-32]. In CALI, intense laser illumination of a chromophore produces deleterious reactive oxygen species that can inactivate a target protein in close proximity (30-45Å) by cleavage or crosslinking of the peptide backbone [13,33-35]. We modified this method to inhibit MyoII function in live *Drosophila* embryos, using the GFP in the MRLC-GFP fusion protein as the target chromophore. In these experiments, MRLC-GFP is expressed in a *sqh* null background so that each MRLC molecule is tagged with GFP. First we asked if we could inhibit cytokinesis, which requires MyoII function. We found that repeated laser illumination of the MRLC-GFP pool on one side of the ingressing furrow in dividing cells inhibits cytokinesis on that side (Fig. 4a, a'). No inhibition was found in similar experiments using Moesin-ABD-GFP, a C-terminal fragment of Moesin fused to GFP which decorates the actin cytoskeleton but has no known cellular function (Fig. 4b, b'). These results show that CALI on MRLC-GFP blocks cytokinesis in live embryos by inhibiting MyoII function with sub-cellular resolution.

To examine the effect of CALI on proteins, we analysed by western-blot single embryos expressing MRLC-GFP, where a large portion of tissue has been subjected to intense laser illumination (Fig. S5a-c). We detect a significant decrease in MRLC-GFP protein levels, whereas levels of the associated MHC, or a nearby membrane protein, such as Dlg, are unaffected. This indicates that the inhibition of MyoII by CALI in our experiments is caused by destruction of MRLC-GFP. No deleterious effects were detected on cell viability or on epithelial integrity (Fig. 4, Fig. S5d, d' and data not shown). Together, these results demonstrate that CALI can inhibit MyoII function efficiently and specifically, with sub-cellular resolution and without detectable cell or tissue toxicity.

We used GFP-based CALI to directly test the requirement of the MyoII cable for cell sorting at PS boundaries. We specifically inhibited the pool of MyoII in the cable by repeated illumination of the PS boundary in *MRLC-GFP* embryos, and then followed the cells' position by time-lapse imaging of the residual GFP fluorescence. We found that when the MyoII cable is inactivated in the presence of dividing boundary cells, the PS boundary is unable to correct cell mixing (100% of cases, n=10), and becomes irregular (IS increases from 1.8±0.3 to 9.6±1.0) (Fig. 5a, d). In these experiments, the pool of MyoII at the cable is the only subcellular pool inactivated, since cytokinesis proceeds normally (Fig. 5e). As a control, we used CALI to target Moesin-ABD-GFP at the PS boundary cable and found that this does not affect the boundary in the presence of cell divisions (IS=3.4±0.3 before CALI and IS=3.6±0.5 after CALI, n=9) (Fig. 5b, d). Since inactivation of MyoII at the cable reproduces the phenotypes found when inhibiting MyoII in the whole tissue, these results suggest that the MyoII cable is responsible for sorting cells at PS boundaries.

We found that the key challenge to embryonic boundaries is the division of boundary cells (Fig. 3) (Note that cells dividing at a distance from the boundary have no effect, Fig. 3a). Consistent with this, CALI inactivation of the MyoII cable in the absence of cell division does not produce cell sorting defects at PS boundaries (IS=2.0±0.6 before CALI and IS=2.6±0.3 after CALI, n=10 in absence of divisions, compared to IS=1.8±0.3 before CALI

and IS=9.6±1.0 after CALI in presence of divisions, n=10) (Fig. 5c, d). Moreover, the MyoII cable is present when the embryonic epithelium is mitotically active, and disappears when divisions cease in the epidermis (Fig. S6). This correlation between mitotic activity and MyoII cabling is also found in the *Drosophila* wing disc. Here, a transient MyoII cable is observed just prior to the formation of a non-proliferative zone at the wing disc D/V boundary [10-12] (Fig. S6). We propose that actomyosin-based barriers function by generating asymmetric tensile forces at the cortex of challenging boundary cells to prevent them from escaping in the opposite compartment, principally when they divide (Fig. 5f).

In conclusion, our results demonstrate that actomyosin barriers sort cells at compartmental boundaries in the early *Drosophila* embryo. MyoII enrichment at the PS boundary interfaces requires Wingless signalling (Fig. 2b), and additional work is required to determine by which mechanism. One possibility is that *wingless* and *engrailed*-expressing cells have different adhesive properties and that this difference triggers MyoII cabling. Supporting this model, mutant clones of the adhesion molecule Echinoid (a Nectin homolog) form actomyosin enrichments at the boundary with wild-type tissue in the *Drosophila* wing disc and follicular epithelium [36,37].

The finding that enrichment of MyoII also occurs at the D/V compartmental boundaries in the *Drosophila* wing disc [10,11] suggests that assembly of actomyosin-based barriers at boundaries could be a general strategy to stop cells with distinct identities from mixing, especially in mitotically active tissues. In the vertebrate hindbrain, Eph/Ephrin signalling regulates cell sorting at rhombomeres boundaries [20,21,26]. Given that Eph/Ephrin signalling regulates the actomyosin cytoskeleton in other contexts such as axonal path finding [38], a role for actomyosin-based barriers could be envisaged in this system.

In developing vertebrate embryos, there is evidence of cell segregation mechanisms not only between compartments, but also between different tissue types [39]. Actomyosin-dependent cortical tension has recently been shown to segregate germ-layers in zebrafish [40]. Together, this and our results suggest that local regulation of cortical tension, rather than differential adhesion, could be the primary mechanism behind cell sorting in living organisms.

MATERIAL & METHODS

Fly strains

The actomyosin cytoskeleton was labelled in live embryos using the following GFP transgenes: *sqh^{AX3}*; *sqh>sqhGFP42* (*MRLC-GFP*) [41], Cyo, *zip^{WeeP181}*-GFP (*MHC-GFP*) [42], *sqh>MoesinABD-GFP* (*Moe-ABD-GFP*, also known as *sGMCA*) [43], *MRLC^{E20E21}* (phospho-mimetic form of MRLC) [44]; *en*>Gal4 [45], *wg*>Gal4 (gift from J.Pradel, Marseilles, France), *arm*>FRT-stop-FRT-Gal4VP16 [46]; KB19 (male specific flipase) [46]; UAS>*GFP-MHC* [47], UAS>*GFP-DN-MHC* [47]. Alleles: *wg^{CX4}* [48], *zip$^{1.3}$* [49], *zip^{1}* [50] and *zip^{2}* [50]. *zip^{CPTI}*-100026 possesses a YFP exon inserted in the head domain of MHC [51] and is a new allele of *zipper* since it does not complement *zip^{1}*, *zip^{2} and zip$^{1.3}$*. *yw* was used as wild-type.

Europe PMC Funders Author Manuscripts

Deficiency screen

The deficiency screen was performed using the molecularly mapped Drosdel chromosomal deficiencies [52]. Stage 9-11 embryos were stained using anti-Engrailed antibody and revealed with an anti-mouse-HRP secondary antibody (Jackson laboratory, 1:200) and DAB staining. Embryos were analysed under a Zeiss Axioplan 2 microscope. We screened for an irregular arrangement of Engrailed nuclei at PS borders.

Immunostainings and antibodies

Embryos are fixed 5 minutes in Heptane:Formaldehyde 37% (1:1). For E-Cad and F-actin, and generally MyoII, embryos were devitellinised manually and stained immediately. Primary antibodies: Mouse anti-Wg (4D4, 1:50), anti-En (4D9, 1:100), anti-Nrt (BP106, 1:5) anti-Dlg (4F3, 1:500) and rat anti-DE-Cad (DCAD2, 1:50) were obtained from DSHB. Rat anti-Ci (2A1, 1:3) is a gift from R.Holmgren [53]. Mouse anti-GFP (cat.#11-814-460-001, 1:50, Roche). Rabbit anti-En (d300, 1:100, Santa Cruz Biotechnology, inc.) and anti-GFP (ab6556, 1:500, Abcam). Secondary antibodies: were either conjugated to Alexa fluorochromes (Alexa 488, Alexa 564 or Alexa 633) and used at 1:500 or to Jackson fluorochromes (TRITC or Cy5) and used at 1:200. F-actin was stained using Phalloidin-Alexa546 (Molecular probes, 1:1000)

Live imaging

Dechorionated embryos are immobilised upon a coverslip with heptane glue and immersed in Voltalef oil (ELF Atochem). Live imaging was performed on a Zeiss LSM510 inverted confocal with 40X or 63X objectives. Projections of Z-stack images were used to generate movies in the software Image J.

Quantification of membrane straightness and assessment of compartmental cell mixing

The index of straightness (IS) is calculated as the difference between measured and minimal theoretical length between two points after normalisation and is expressed in arbitrary units (A.U.). 1A.U. means that the measured length is 1% longer than the straight line. Membrane length is measured with the software Image J. We measured, in absence of cell division (except for Fig. 3c'), the length of membrane interfaces for PS boundary cells or for other columns of cells,.

In fixed embryos, membrane interfaces corresponding to PS boundaries were identified by Engrailed expression. Measures were performed on confocal sections corresponding to the plane of the adherens junctions (AJs). Images were captured at random locations along AP and DV axes in the embryo trunk, using a 40X objective and a numerical zoom 4 on a Zeiss LSM510 confocal. Images shown correspond to a superposition of E-Cad staining at the AJs (usually one confocal section) and a projection of all Z sections for En staining. Note that we systematically went through the whole stack of Z sections in these double stainings in order to accurately identify the interfaces corresponding to the PS boundary.

In live embryos, including in CALI experiments, PS boundaries were identified by MyoII or Moesin-ABD-GFP enrichment. Images were taken with a 63X objective and a numerical zoom 3 on a Zeiss LSM510 confocal.

In experimental cases where the PS boundary was irregular compared to wild-type, some cells may be displaced into the adjacent compartment. We consider that these are events of compartmental cell mixing when the displaced cell has less junctional contacts with cells with the same identity than with cells with a different identity.

Injection of the ROCK inhibitor Y-27632

Stage 8-9 embryos of the indicated genotype were injected in the yolk at room temperature with 1 mM Y-27632 (TOCRIS) or dH_2O in control experiments. Embryos were aged for 30 min at 25°C, fixed and stained using standard procedures.

Since loss of epithelial integrity leads to massive cell dispersal in the early *Drosophila* embryo [54], we systematically checked epithelial integrity using E-Cad staining in loss-of-function experiments. Regarding Y-27632, 1mM is the highest concentration that can be used without affecting the epithelium integrity. At this concentration, some cell divisions still occur.

Western blots on single embryos and quantification of protein levels

We have used two protocols for Western blots: one including a fixation step for GFP and Phospho-MRLC, another without fixation for MHC. GFP and Dlg works in both conditions. Single embryos glued on a coverslip are detached by soaking them briefly in heptane. If fixation is required, embryos are transferred in fixative solution (formaldehyde 37%: heptane (1:1)) and fixed for 5 minutes, thoroughly rinsed with PBS 1X Triton 0.1% and hand devitellinised in PBS. 5 to 10 embryos are pooled in 100-200µl Laemli buffer: PBS 1X (1:1) and boiled for 5 minutes. Should fixation be avoided, embryos are thoroughly rinsed with PBS 1X Triton 0.1%, transferred in 20µl Laemli buffer: PBS 1X (1:1), carefully crushed with a needle and boiled for 5 minutes.

The equivalent of one embryo is loaded per lane. Standard procedures are used for Western blot analysis. Revelation is performed using ECL Standard Plus kit (Perkin Elmer Life Science). Primary antibodies: mouse anti-Dlg (1:300, DSHB) and anti-GFP (1:500, Roche), rabbit anti-Phospho-MRLC (Phospho-Ser19, cat.#3671, 1:100, CST) and anti-MHC (#656, 1/10000) [55]. Secondary antibodies: mouse or rabbit HRP-conjugated (1:2000, Jackson Laboratories).

Films were scanned and quantification of protein levels was performed using Image J. Since there is no significant difference in Dlg protein levels between control and CALI-treated embryos (n=13) (which is consistent with Dlg being unaffected when examining immunofluorescence levels in whole embryos (Fig. S5d, d')), we used Dlg as a loading control to normalise protein levels for GFP, phospho-MRLC and MHC.

Statistical analyses—Data from all quantifications are reported as mean ± SEM. The significance between groups of data was assessed by unpaired Student's t test (Fig.1d) or by paired Student's t test (Fig.1d, boundary *vs* D/V junctions in WT; Fig. 2c; Fig. 5d; Fig. S5b). Results are considered significant with p less than 0.05 (*p<0.05, **p<0.02, ***p<0.001).

Chromophore-Assisted Laser Inactivation (CALI)

GFP was used as a chromophore to perform CALI on two fusion proteins, MRLC-GFP [41] and the control Moesin-ABD-GFP [43]. MRLC-GFP was used in a null background mutant for *spaghetti-squash*. The control Moesin-ABD-GFP which corresponds to the actin-binding domain of Moesin that decorates F-actin, is expressed in a wild-type background. CALI is performed using either an inverted or an upright LSM510 laser-scanning confocal microscope (Zeiss) with a Lasos 50 mW Argon laser set at 50% of its power. For image acquisition, GFP is excited using the 488 nm laserline at 1-3%. For CALI itself, in order to excite GFP maximally and hence to locally produce highest levels of reactive oxygen species, both 477 nm and 488 nm laserlines set at 100% were used. Depending on the experiment, we used a Plan-Apochromat 63X/1.4 Oil DIC objective or a Plan-Neofluar 40X/1.3 Oil DIC objective (Zeiss).

CALI conditions for assessment of protein integrity by Western blot and immunostaining

CALI was performed during dorsal closure on the dorsal side of *MRLC-GFP* embryos by continuous scanning of a Region Of Interest (ROI) during 5 minutes. Protein levels were then analysed by Western blots or whole-mount immunostainings. For Western blot analysis, we used the 63x objective and a 0.7X numerical zoom. We scanned a ROI of 200 μm x 120 μm (which roughly covers the trunk of the embryo) for 21 μm in depth (15 sections every 1.5 μm). Parameters are: pixel time: 12.8 μs; scan time: 798.91 ms; scan speed: 5; number of scanning per frame: 1; pinhole: 3.37 Airy units. For immunostaining analysis, we used a 40X objective and a 0.7X numerical zoom. We scanned a ROI of 90 μm x 50 μm for 12 μm in depth (9 sections every 1.5 μm). Parameters are: pixel time: 6.39 μs; scan time: 552.44 ms; scan speed: 6; number of scanning per frame: 2; pinhole: 0.93 Airy unit. As soon as CALI is completed, embryos were individually processed for Western blot or immunostaining experiments (see above).

CALI conditions for MyoII inhibition during cytokinesis

CALI is performed on ectodermal dividing cells on stage 9/10 *MRLC-GFP* (or *Moesin-ABD-GFP)* embryos using the 40X objective and a 5X numerical zoom. We used laser pulses (6-8 sec) followed by acquisition of ten images (one every second). Parameters, based on the LSM510 Frap module (Zeiss), are: pixel time: 1.60 μs; scan speed: 9; number of scanning per frame: 1; pinhole: 0.93 Airy unit; iterations: 10. The cytokinesis ring is targeted at only one focal plane with an average ROI of 5 μm x 2 μm. If needed, the ROI is slightly shifted during the experiment to follow the cytokinesis ring. The opposite side of the cytokinesis ring is taken as an internal control.

CALI conditions for MyoII inhibition at the PS cable

CALI was performed on stage 9/early stage 10 *MRLC-GFP* (or *Moesin-ABD-GFP*) embryos using the 63X objective and a 3X numerical zoom. A cycle (1 laser pulse + 1 acquisition) lasts 6-9 seconds, depending of the ROI size. The PS boundary is targeted at only one focal plane with a ROI of 3 μm x 20 μm in average. If needed, the ROI is slightly shifted in X, Y and/or Z axis during the experiment to follow the PS boundary. CALI was performed during 1 to 10 minutes on boundary cells prior division. Parameters, based on the LSM510 Frap

module (Zeiss), are: pixel time: 2.56 μs; scan speed: 8; number of scanning per frame: 1; pinhole: 3.37 Airy units; iterations: 3. We acquired one image prior each CALI experiment as a reference. During and after CALI, cells are tracked by time-lapse microscopy using residual GFP fluorescence. Modification of membrane straightness is measured only in the targeted area, at AJs level and once challenging divisions are completed.

Supplementary Material

Refer to Web version on PubMed Central for supplementary material.

Acknowledgments

We thank Nicola Lawrence for the initial observation of the segmental pattern of MyoII cables and for movie S1; Bita Bordbar for her help in screening chromosomal deficiencies; D. Kiehart, R. Karess, G. Davis, J. Pradel, R. Holmgren, Cambridge Protein Trap Insertion Consortium, Bloomington Stock Centre and the Developmental Studies Hybridoma Bank for reagents. We thank B. Harris, R. Keynes, L. Perrin, M. Sémériva and D. St Johnston for critical reading of the manuscript. This work was funded by HFSP and Wellcome Trust grants to B.S; a Wellcome Trust Program Grant to A.H.B; an EMBO fellowship to A.P-M and an ARC (Association pour la Recherche contre le Cancer) and Herchel Smith fellowships to B.M.

REFERENCES

1. Dahmann C, Basler K. Compartment boundaries: at the edge of development. Trends Genet. 1999; 15(8):320–326. [PubMed: 10431194]
2. Irvine KD, Rauskolb C. Boundaries in development: formation and function. Annu Rev Cell Dev Biol. 2001; 17:189–214. [PubMed: 11687488]
3. Tepass U, Godt D, Winklbauer R. Cell sorting in animal development: signalling and adhesive mechanisms in the formation of tissue boundaries. Current opinion in Genetics & Development. 2002; 12(5):572–582. [PubMed: 12200163]
4. Dahmann C, Basler K. Opposing transcriptional outputs of Hedgehog signaling and Engrailed control compartmental cell sorting at the Drosophila A/P boundary. Cell. 2000; 100(4):411–422. [PubMed: 10693758]
5. Garcia-Bellido A, Ripoll P, Morata G. Developmental compartmentalisation of the wing disk of Drosophila. Nat New Biol. 1973; 245(147):251–253. [PubMed: 4518369]
6. Inoue T, et al. Role of cadherins in maintaining the compartment boundary between the cortex and striatum during development. Development. 2001; 128(4):561–569. [PubMed: 11171339]
7. Milan M, Weihe U, Perez L, Cohen SM. The LRR proteins Capricious and Tartan mediate cell interactions during DV boundary formation in the Drosophila wing. Cell. 2001; 106(6):785–794. [PubMed: 11572783]
8. Schlichting K, Demontis F, Dahmann C. Cadherin Cad99C is regulated by Hedgehog signaling in Drosophila. Dev Biol. 2005; 279(1):142–154. [PubMed: 15708564]
9. Vegh M, Basler K. A genetic screen for hedgehog targets involved in the maintenance of the Drosophila anteroposterior compartment boundary. Genetics. 2003; 163(4):1427–1438. [PubMed: 12702686]
10. Major RJ, Irvine KD. Influence of Notch on dorsoventral compartmentalization and actin organization in the Drosophila wing. Development. 2005; 132(17):3823–3833. [PubMed: 16049109]
11. Major RJ, Irvine KD. Localization and requirement for Myosin II at the dorsal-ventral compartment boundary of the Drosophila wing. Dev Dyn. 2006; 235(11):3051–3058. [PubMed: 17013876]
12. O'Brochta DA, Bryant PJ. A zone of non-proliferating cells at a lineage restriction boundary in Drosophila. Nature. 1985; 313(5998):138–141. [PubMed: 3917556]

13. Jacobson K, Rajfur Z, Vitriol E, Hahn K. Chromophore-assisted laser inactivation in cell biology. Trends Cell Biol. 2008; 18(9):443–450. [PubMed: 18706812]
14. Jay DG. Selective destruction of protein function by chromophore-assisted laser inactivation. Proc Natl Acad Sci U S A. 1988; 85(15):5454–5458. [PubMed: 3399501]
15. Davy A, Bush JO, Soriano P. Inhibition of gap junction communication at ectopic Eph/ephrin boundaries underlies craniofrontonasal syndrome. PLoS Biol. 2006; 4(10):1763–1776.
16. Perez-Pomares JM, Foty RA. Tissue fusion and cell sorting in embryonic development and disease: biomedical implications. Bioessays. 2006; 28(8):809–821. [PubMed: 16927301]
17. Twigg SR, et al. Mutations of ephrin-B1 (EFNB1), a marker of tissue boundary formation, cause craniofrontonasal syndrome. Proc Natl Acad Sci U S A. 2004; 101(23):8652–8657. [PubMed: 15166289]
18. Blair SS, Ralston A. Smoothened-mediated Hedgehog signalling is required for the maintenance of the anterior-posterior lineage restriction in the developing wing of Drosophila. Development. 1997; 124(20):4053–4063. [PubMed: 9374402]
19. Cheng YC, et al. Notch activation regulates the segregation and differentiation of rhombomere boundary cells in the zebrafish hindbrain. Dev Cell. 2004; 6(4):539–550. [PubMed: 15068793]
20. Cooke JE, Kemp HA, Moens CB. EphA4 is required for cell adhesion and rhombomere-boundary formation in the zebrafish. Curr Biol. 2005; 15(6):536–542. [PubMed: 15797022]
21. Mellitzer G, Xu Q, Wilkinson DG. Eph receptors and ephrins restrict cell intermingling and communication. Nature. 1999; 400(6739):77–81. [PubMed: 10403252]
22. Milan M, Cohen SM. A re-evaluation of the contributions of Apterous and Notch to the dorsoventral lineage restriction boundary in the Drosophila wing. Development. 2003; 130(3): 553–562. [PubMed: 12490561]
23. Morata G, Lawrence PA. Control of compartment development by the engrailed gene in Drosophila. Nature. 1975; 255(5510):614–617. [PubMed: 1134551]
24. Rodriguez I, Basler K. Control of compartmental affinity boundaries by hedgehog. Nature. 1997; 389(6651):614–618. [PubMed: 9335503]
25. Shen J, Dahmann C. The role of Dpp signaling in maintaining the Drosophila anteroposterior compartment boundary. Dev Biol. 2005; 279(1):31–43. [PubMed: 15708556]
26. Xu Q, Mellitzer G, Robinson V, Wilkinson DG. In vivo cell sorting in complementary segmental domains mediated by Eph receptors and ephrins. Nature. 1999; 399(6733):267–271. [PubMed: 10353250]
27. Sanson B. Generating patterns from fields of cells: examples from Drosophila segmentation. EMBO Rpts. 2001; 2(12):1083–1088.
28. Vincent JP, O'Farrell PH. The state of engrailed expression is not clonally transmitted during early Drosophila development. Cell. 1992; 68(5):923–931. [PubMed: 1547492]
29. Zallen JA, Wieschaus E. Patterned gene expression directs bipolar planar polarity in Drosophila. Dev Cell. 2004; 6(3):343–355. [PubMed: 15030758]
30. Rajfur Z, Roy P, Otey C, Romer L, Jacobson K. Dissecting the link between stress fibres and focal adhesions by CALI with EGFP fusion proteins. Nat Cell Biol. 2002; 4:286–293. [PubMed: 11912490]
31. Diefenbach TJ, et al. Myosin 1c and myosin IIB serve opposing roles in lamellipodial dynamics of the neuronal growth cone. J Cell Biol. 2002; 158(7):1207–1217. [PubMed: 12356865]
32. Wang FS, Wolenski JS, Cheney RE, Mooseker MS, Jay DG. Function of myosin-V in filopodial extension of neuronal growth cones. Science. 1996; 273(5275):660–663. [PubMed: 8662560]
33. Horstkotte E, Schroder T, Niewohner J, Jay DG, Henning SW. Toward understanding the mechanism of chromophore-assisted laser inactivation - evidence for the primary photochemical steps. Photochem Photobiol. 2005; 81:358–366. [PubMed: 15623352]
34. Liao JC, Roider J, Jay DG. Chromophore-assisted laser inactivation of proteins is mediated by the photogeneration of free-radicals. Proc Natl Acad Sci U S A. 1994; 91:2659–2663. [PubMed: 8146171]

35. Yan P, et al. Fluorophore-assisted light inactivation of Calmodulin involves singlet-oxygen mediated cross-linking and methionine oxidation. Biochemistry. 2006; 45:4736–4748. [PubMed: 16605242]
36. Laplante C, Nilson LA. Differential expression of the adhesion molecule Echinoid drives epithelial morphogenesis in Drosophila. Development. 2006; 133(16):3255–3264. [PubMed: 16854971]
37. Wei SY, et al. Echinoid is a component of adherens junctions that cooperates with DE-Cadherin to mediate cell adhesion. Dev Cell. 2005; 8(4):493–504. [PubMed: 15809032]
38. Huber AB, Kolodkin AL, Ginty DD, Cloutier J.-F.o. SIGNALING AT THE GROWTH CONE: Ligand-Receptor Complexes and the Control of Axon Growth and Guidance. Annual Review of Neuroscience. 2003; 26(1):509–563.
39. Townes PL, Holtfreter J. Directed movements and selective adhesion of embryonic amphibian cells. J Exp Zool. 1955; 128:53–120.
40. Krieg M, et al. Tensile forces govern germ-layer organization in zebrafish. Nat Cell Biol. 2008; 10(4):429–436. [PubMed: 18364700]
41. Royou A, Sullivan W, Karess R. Cortical recruitment of nonmuscle myosin II in early syncytial Drosophila embryos: its role in nuclear axial expansion and its regulation by Cdc2 activity. J Cell Biol. 2002; 158(1):127–137. [PubMed: 12105185]
42. Clyne PJ, Brotman JS, Sweeney ST, Davis G. Green fluorescent protein tagging Drosophila proteins at their native genomic loci with small P elements. Genetics. 2003; 165(3):1433–1441. [PubMed: 14668392]
43. Kiehart D, Galbraith C, Edwards K, Rickoll W, Montague R. Multiple forces contribute to cell sheet morphogenesis for dorsal closure in Drosophila. J Cell Biol. 2000; 149(2):471–490. [PubMed: 10769037]
44. Winter CG, et al. Drosophila Rho-associated kinase (Drok) links Frizzled-mediated planar cell polarity signaling to the actin cytoskeleton. Cell. 2001; 105(1):81–91. [PubMed: 11301004]
45. Brand AH, Perrimon N. Targeted gene expression as a means of altering cell fates and generating dominant phenotypes. Development. 1993; 118(2):401–415. [PubMed: 8223268]
46. Sanson B, White P, Vincent JP. Uncoupling cadherin-based adhesion from wingless signalling in Drosophila. Nature. 1996; 383(6601):627–630. [PubMed: 8857539]
47. Franke J, Montague R, Kiehart D. Nonmuscle Myosin II generates forces that transmit tension and drive contraction in multiple tissues during dorsal closure. Current Biology. 2005; 15:2208–2221. [PubMed: 16360683]
48. Baker NE. Molecular cloning of sequences from wingless, a segment polarity gene in Drosophila: the spatial distribution of a transcript in embryos. EMBO J. 1987; 6(6):1765–1773. [PubMed: 16453776]
49. Young PE, Richman AM, Ketchum AS, Kiehart DP. Morphogenesis in Drosophila requires nonmuscle myosin heavy chain function. Genes Dev. 1993; 7(1):29–41. [PubMed: 8422986]
50. Tearle RG, Nusslein-Volhard C. Tubingen mutants and stock list. 1987; Vol. 66:209–269.
51. Cambridge Protein Trap Insertion Consortium. Russell, S.; St Johnston, D. unpublished
52. Ryder E, et al. The DrosDel deletion collection: a Drosophila genomewide chromosomal deficiency resource. Genetics. 2007; 177(1):615–629. [PubMed: 17720900]
53. Motzny CK, Holmgren R. The Drosophila cubitus interruptus protein and its role in the wingless and hedgehog signal transduction pathways. Mech Dev. 1995; 52(1):137–150. [PubMed: 7577671]
54. Chandraratna D, Lawrence N, Welchman DP, Sanson B. An in vivo model of apoptosis: linking cell behaviours and caspase substrates in embryos lacking DIAP1. Journal of Cell Science. 2007; 120:2594–2608. [PubMed: 17636001]
55. Kiehart DP, Feghali R. Cytoplasmic myosin from Drosophila melanogaster. J Cell Biol. 1986; 103(4):1517–1525. [PubMed: 3095337]

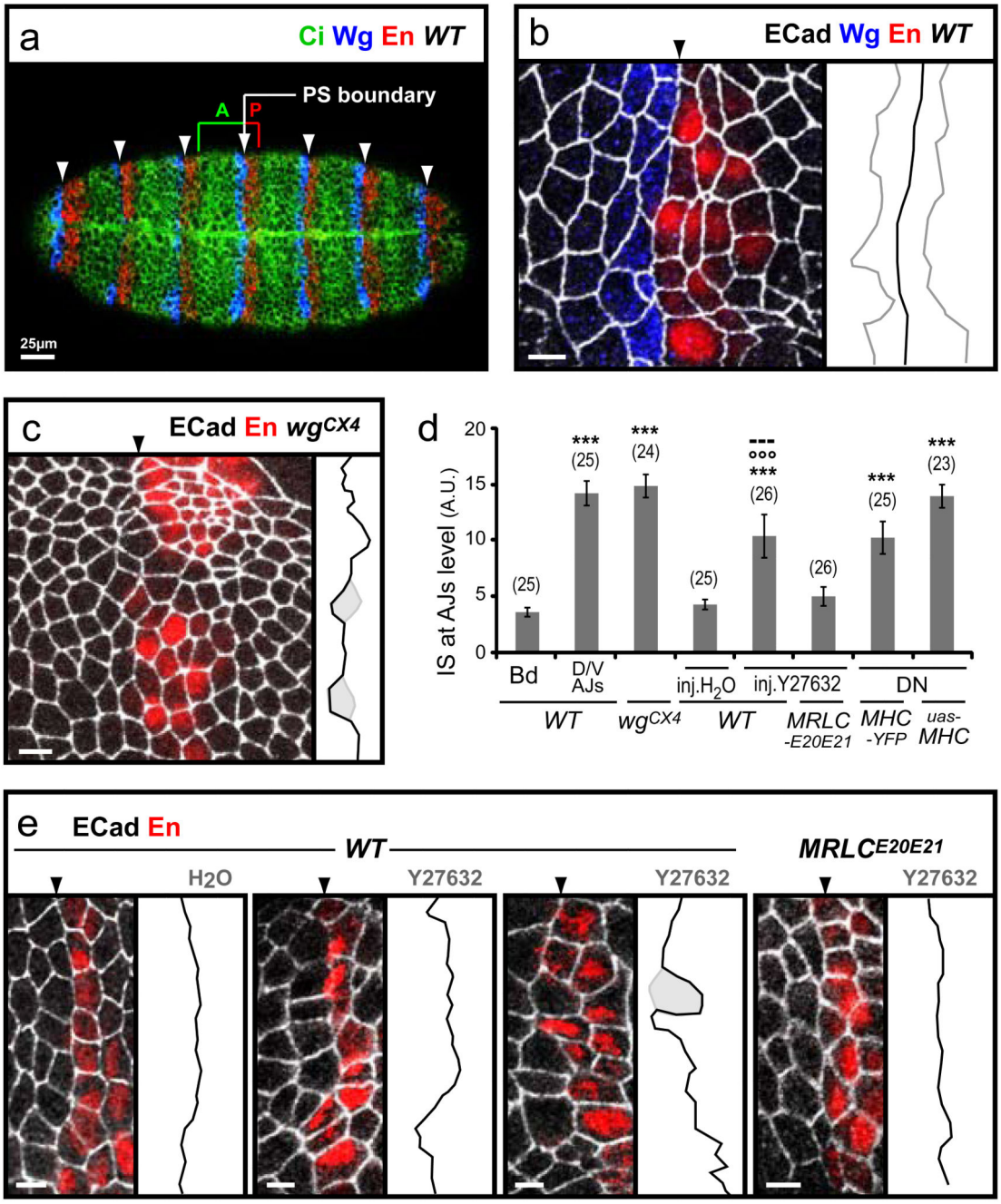

Fig. 1. Myosin II is required for cell sorting at lineage restriction boundaries in *Drosophila* embryos

(a) Ventral view of an early *Drosophila* embryo showing expression of Wingless (Wg), Engrailed (En) and Cubitus interuptus (Ci). The parasegmental (PS) boundaries form at the interface of Wg and En stripes (arrowheads), where anterior (A) and posterior (P) compartments meet. (b) Close-up of the epithelium (scale bars here and subsequent panels correspond to 5µm), with E-Cadherin stain (E-Cad, white) highlighting the adherens junctions (AJ). Membrane interfaces at the PS boundary (arrowhead) are arranged in a straight line (extracted in black on the right-hand side), in contrast to other columns of

interfaces that are not PS boundaries (examples extracted in grey). (c) In a wg^{CX4} mutant embryo, absence of Wg expression leads to loss of En expression and breakdown of compartmentalisation. Transient initial En expression allows one to identify the membrane interfaces where PS boundaries would have formed: these interfaces are not aligned and some cells (highlighted in grey) invade what would have been the neighbouring compartment. (d) Index of Straightness quantification (IS, see Material and Methods) confirming that in wild-type (WT), membrane interfaces are straighter at PS boundaries (Bd) compared to non-PS boundary interfaces (D/V AJs). PS boundaries lose their straightness in absence of compartmentalisation (wg^{CX4}) or when Myosin II (MyoII) function is inhibited by either injection of drug Y27632 (see e) or expression of dominant-negative constructs (DN, see Fig. S2). The numbers of boundaries measured are indicated in parentheses (In average, 2-3 boundaries are analysed per embryo). Data are expressed as mean ± SEM. The symbol * indicates a statistical comparison with IS at PS boundaries in *WT* using Student's t test, with *** corresponding to $p<0.001$. °°° and $^{---}$ indicate a comparison with *WT* embryos after H_20 injection, and with $MRLC^{E20E21}$ embryos after Y27632 injection, respectively. (e) In contrast to the control injection of H_2O in *WT* embryos, injection of 1 mM Y27632 leads to irregular PS boundaries, with cells occasionally invading the adjacent compartment (highlighted in grey). When Y27632 is injected in embryos expressing $MRLC^{E20E21}$, a phospho-mimetic form of MRLC, the boundary defects are fully rescued.

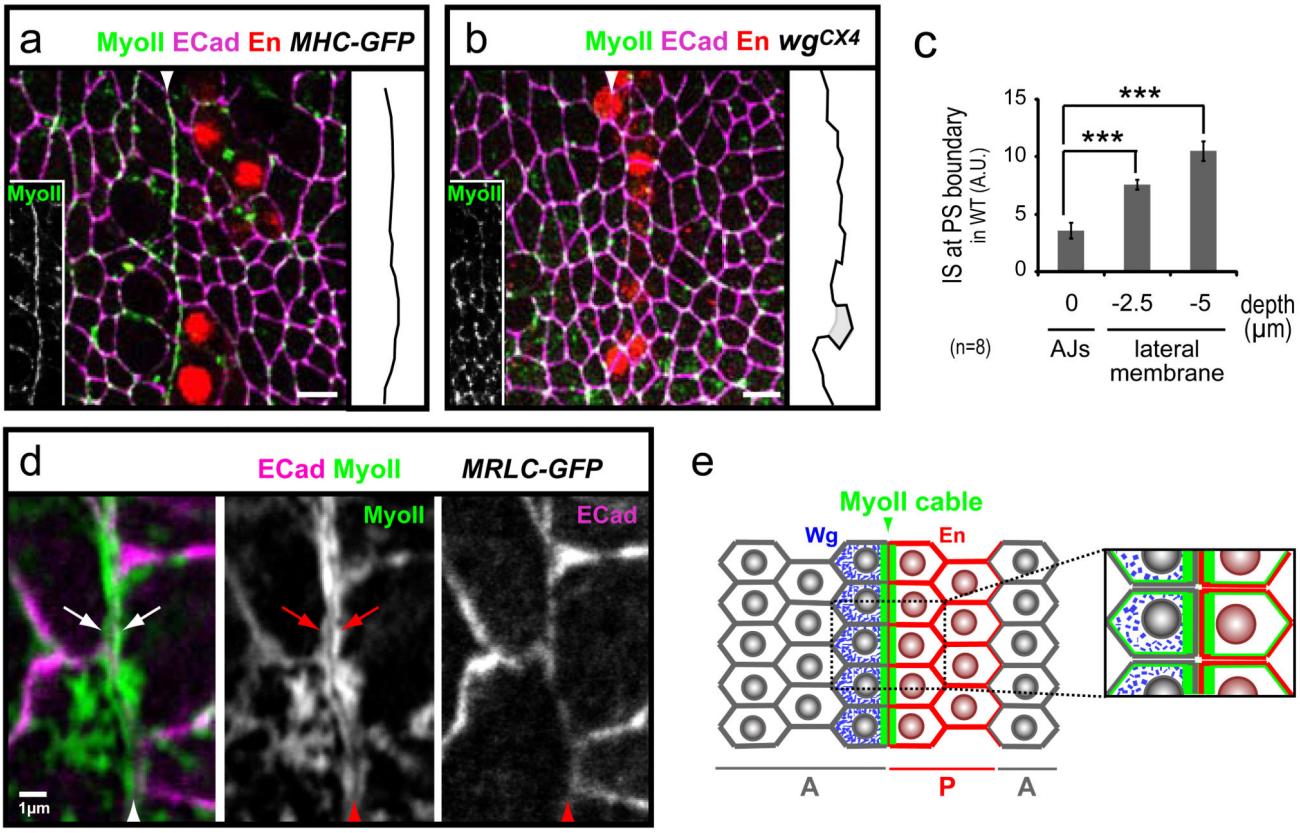

Fig. 2. An actomyosin cable forms at the PS boundary

All scale bars represent 5µm. (a) Top view of the epidermis showing a confocal section at the level of AJs: MyoII is enriched in a cable-like structure at the membrane interfaces corresponding to the PS boundary. (b) In absence of compartmentalisation in *wg*^{CX4} embryos, MyoII does not form a cable where PS boundaries would have formed, but MyoII localisation at AJs is unaffected. (c) IS at PS boundaries along the apical/basal axis in wild-type embryos: membranes are aligned at the AJs, but lose their alignment 2.5 and 5 µm basal to the AJs (n=8). Data are expressed as mean ± SEM. The symbol * indicates a statistical comparison between IS measured at the level of AJs and at the level of the lateral membranes, using paired Student's t test and with *** corresponding to $p<0.001$. (d) Magnified view of the PS boundary in *MRLC-GFP* embryos: MyoII is enriched at the cortex of both anterior and posterior boundary cells (arrows), on either side of the two apposed plasma membranes labelled by E-Cad staining. (e) Schema of MyoII enrichment at a PS boundary.

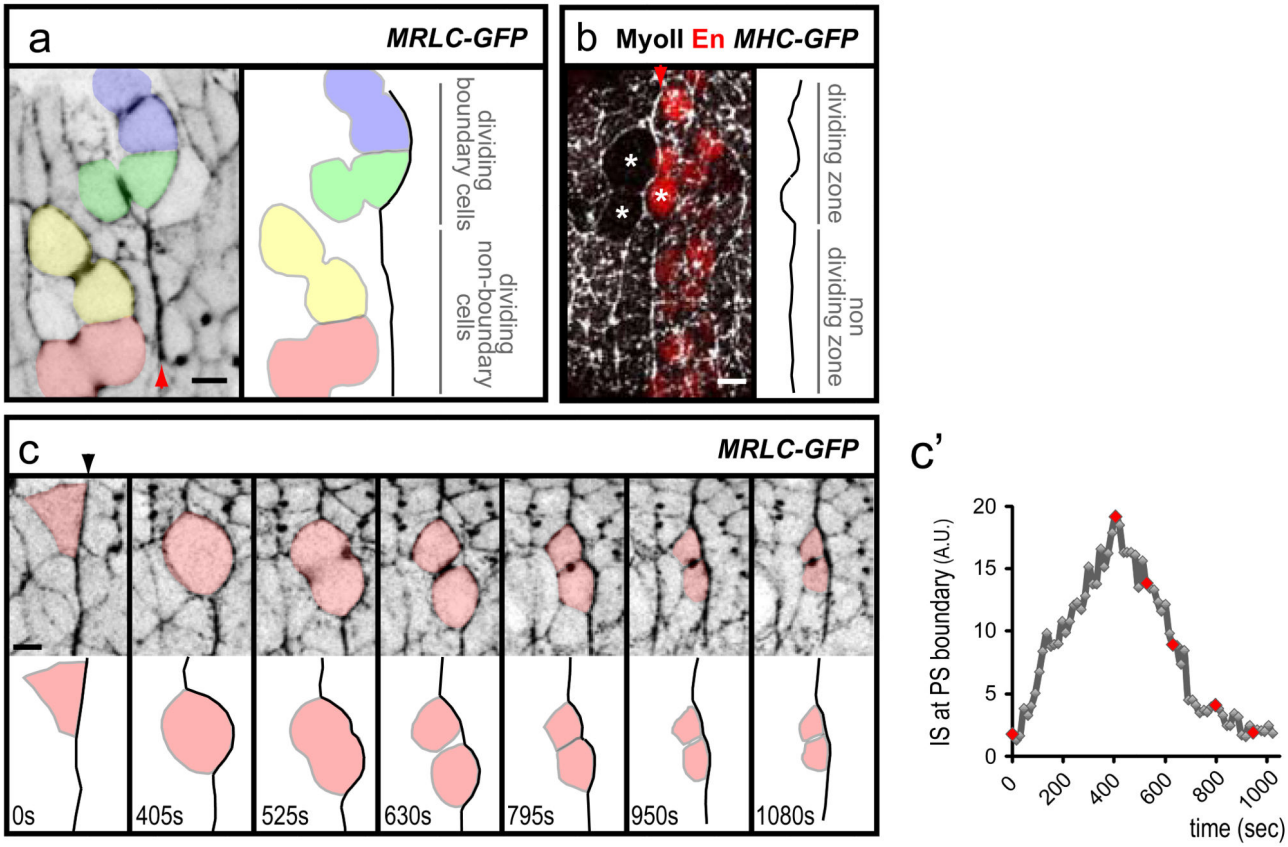

Fig. 3. Cell divisions challenge PS boundaries

(a) Movie frame showing that dividing boundary cells (coloured blue and green), but not non-boundary cells (red and yellow) deform the MyoII cable at a PS boundary (identified by $MRLC^{GFP}$ enrichment, arrowhead). (b) The MyoII cable (arrowhead) is not dismantled when boundary cells divide (stars). (c) Movie frames of a *MRLC-GFP* embryo showing how the division of a boundary cell deforms transiently the MyoII cable (identified by $MRLC^{GFP}$ enrichment). c') Quantification of membrane straightness for the first 6 frames in c (red dots). Note that, in contrast to all other quantifications which consider several boundary cells, the IS measured here corresponds to the length of the interface of the boundary cell coloured in red.

Europe PMC Funders Author Manuscripts

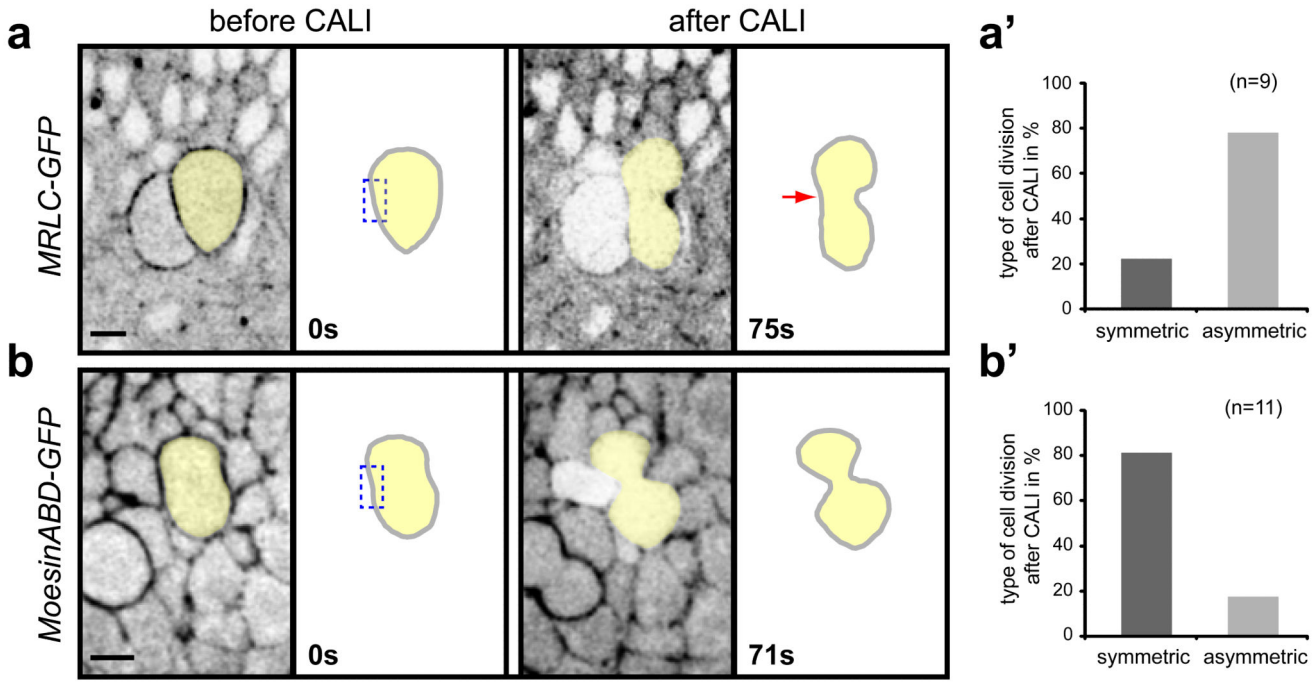

Fig. 4. CALI inactivation of MyoII blocks cytokinesis

Movie frames showing that CALI performed on one side (dashed box) of the cytokinesis ring in dividing epithelial cells impairs membrane invagination (red arrow) in *MRLC-GFP* embryos (a), but has no effect in *Moesin-ABD-GFP* embryos (b). Membrane invagination is delayed in *MRLC-GFP* embryos a few seconds after the beginning of CALI. (a', b') Quantifications of asymmetric (membrane invagination impaired on one side) versus symmetric divisions after CALI in *MRLC-GFP* (a') or *Moesin-ABD-GFP* (b').

Europe PMC Funders Author Manuscripts

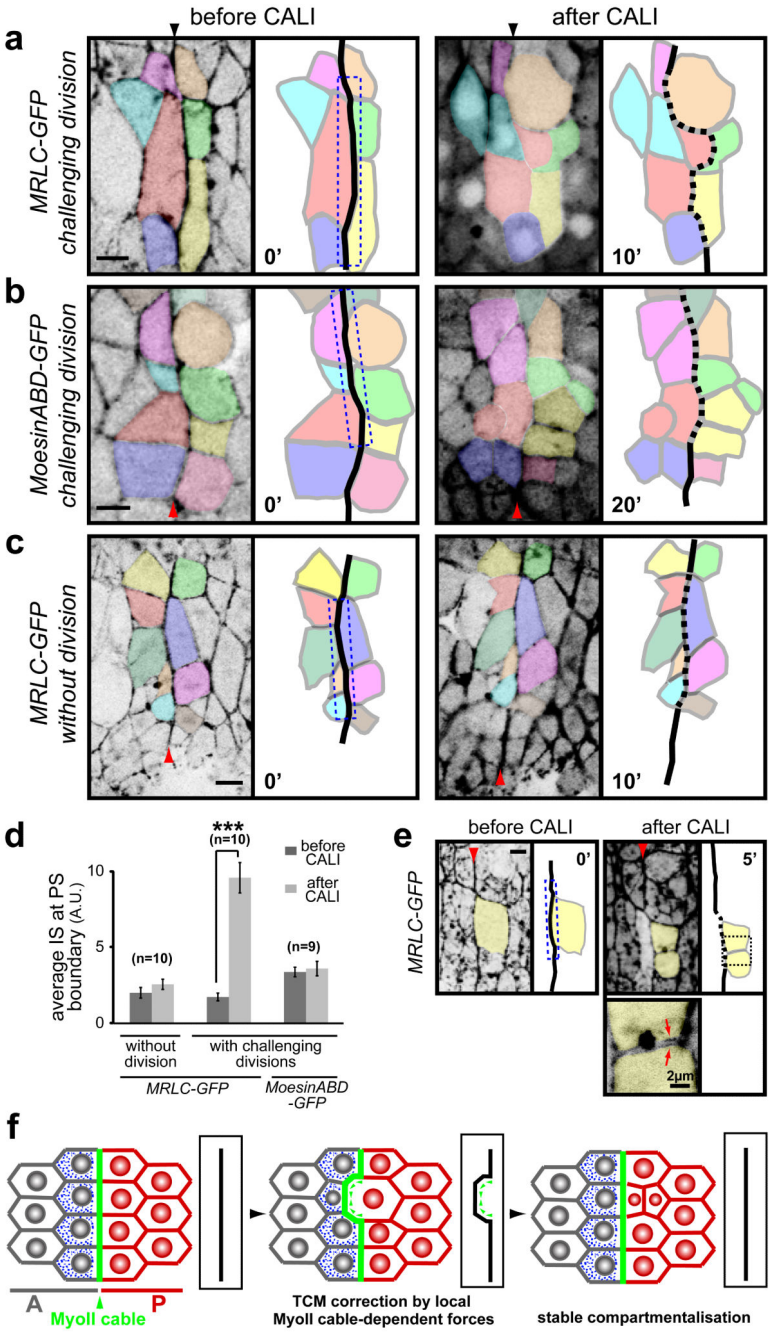

Fig. 5. CALI inactivation of the MyoII cable gives cell sorting defects at PS boundaries

(a-c) Movie frames showing CALI performed on the PS boundary (dashed box) in embryos expressing *MRLC-GFP* (a, c) or *Moesin-ABD-GFP* (b). (a) In presence of the division of an anterior boundary cell (coloured in red), CALI inactivation of MyoII at the cable leads to an irregular PS boundary (dashed). After division, one daughter cell invades the posterior compartment. (b) A similar experiment in *Moesin-ABD-GFP* control embryos does not affect cell sorting at the boundary, even after four of the boundary cells have divided. (c) CALI targeting of the MyoII cable in *MRLC-GFP* embryos in absence of divisions: no cell

sorting defects are observed in those conditions. (d) Quantification of membrane straightness after CALI at PS boundaries, in presence and absence of boundary cell divisions. Data are expressed as mean ± SEM. The symbol * indicates a statistical comparison between conditions before and after CALI in the indicated contexts, using paired Student's t test and with *** corresponding to $p<0.001$. (e) Cable inactivation (dashed box) does not affect the MyoII pool required for division of the targeted boundary cell (yellow), since the cytokinesis ring forms and the cell divides normally (panel 5′). Arrows on the close-up view show MyoII localising at the cortex of the newly formed membranes within each daughter cells. (f) Model of cell sorting at *Drosophila* embryonic lineage restriction boundaries. TCM: transient cell mixing.